Getting 3D Facial Image Distortion Using Pincushion Deformations

Cahyo Darujati[†,††], Bimo Gumelar[††], Supeno Mardi[†,†††], and Mochamad Hariadi[†,†††]

[†] Department of Electrical Engineering, Institut Teknologi Sepuluh Nopember (ITS) Surabaya, Indonesia
[††]Faculty of Computer Science, Narotama University, Surabaya, Indonesia
[†††] Department of Computer Engineering, Institut Teknologi Sepuluh Nopember (ITS), Surabaya, Indonesia

Summary
In computer graphics, techniques for manipulation, deformation, and animation are merely close and often inter-related, and in deformation modeling, we need some smooth shapes without discontinuities. In this paper, we experiment in the context of manipulation for deformation modeling process. All these operations can be an option to serve as building characters of animation. For the moment, while the literature on deformation and animation are dominated by surface-based modeling and rendering techniques, we consider techniques that are designed to transform the geometrical shape and general overview of the scopes of deformation. Simulation results demonstrate the algorithms developed to apply distortion of them fulfills all the requirements of image data. By utilizing this kind of the most common form effect, lens distortion, which is a nonlinear and generally radial distortion. We generate our 3D facial image using pincushion distortion. The pincushion distortion is an opposite effect when the edges are magnified stronger. In this experiment, the process is based on shifting pixels which may cause aliasing, and by the end of our experiment, we get some common problem of distorting computer-generated images; there are black areas at the border.

Keywords:
3d facial image, pincushion deformation, deformation modeling

1. Introduction

As a various modeling and animation tasks such a character animation, there have recently been some works on domain-based deformation. Moreover, many techniques on image deformation methods have arisen much interest in image animation, image reconstruction, and image analysis. Image deformation is an image processing technique, which creates smooth and realistic deformation results based on deformation control features and specific deformation functions. This technique is often used in computer animation and medical image processing. Variously the deformations methods using traditional image deformation algorithms often giving lack from realism. From accurate of the human facial and character representation, human face are similar in any ways on both structure and its shape. 3D deformation is useful for various modeling and animation tasks such as surface sculpting and character animation. There have recently been some works on gradient-domain mesh based deformation [2, 12, 13]. Such methods are capable of preserving local surface details during editing, and is usually "global" in the sense that the algorithms explicitly scatters the desired deformation, often specified on a set of handle vertices, across the entire mesh, usually through least-square solving a large sparse linear system connecting every pair of neighboring mesh elements. Huang et al. [2] further introduce a non-linear optimizing framework, allowing the incorporation of various non-linear constraints such as rigidity constraint and volume constraint.

2. Theoretical Principles

In the 3D facial data, the tip of the nose can be detected reliably. Therefore, we regard this point as the reference point and calculate the geodesic distance from it to other points. Since all the points are centered around the nose tip and the geodesic distance is in the radial direction, it is called as radial geodesic distance. The computation of this kind of distance is described as following by two given points as a surface curve between, then can be described as shown in Equation 1.

$$l(t) = (x(t), y(t), z(t)) . \quad (1)$$

Where x(t) and y(t) refer to the position in the X-Y plane and z(t) refers to the corresponding depth value. The geodesic length d of this curve is given by Equation 2.

$$\mathrm{d} = \int_{\mathrm{a}}^{\mathrm{b}} \sqrt{\mathrm{x}_{\mathrm{t}}^2 + \mathrm{y}_{\mathrm{t}}^2 + \mathrm{z}_{\mathrm{t}}^2}\,\mathrm{dt} . \quad (2)$$

where the subscripts denote partial derivatives, e.g. $x_t = \frac{dx}{dt}$

Most models formulate the problem as an energy optimization problem, which simultaneously minimizes the appearance similarity term while satisfying some manually defined smooth constraints to keep the continuity and such constraints cannot handle large and complex deformations very well, and hence the models will fail to keep the structure of the distorted object [14]. While the other

Manuscript received August 5, 2018
Manuscript revised August 20, 2018

objects including many different properties could react in many ways of deformation. The object models cannot describe different structural changes of its objects. The object models cannot address exact correspondence of local features.

2.1 Free-Form Deformation (FFD)

Free-form deformation (FFD) is a popular modeling method for stable geometries and also flexible modeling tool for wireframe surfaces and polygonal data images. This method involves a user that allows modifying the shape of an object by picking and dragging control points. In the 3D computer graphics research area, it coupled with the step towards simplifying the interface of 3D modeling. A 3D object, usually represented as a polygonal mesh, is surrounded by a lattice of control vertices. As the user displaces the points in the control lattice, the vertices of the polygon mesh are proportionally displaced as well. This proven technique works very well for many applications. However, setting up the FFD lattice and moving its control points to the desired positions can be a cumbersome, time-consuming process. Barr [15] was presented the current technique of geometric deformation; it was constrained and limited to operations at the single axis and by only a few parameters to modification. FFD, as we know it today, was developed by Parry and Sederberg in [16]. In FFD, a geometric model is enclosed within a parallelepiped lattice of control vertices. Any point X on the model with Cartesian coordinates in world space has corresponding (s,t,u) coordinates in lattice space as shown in Figure 1.

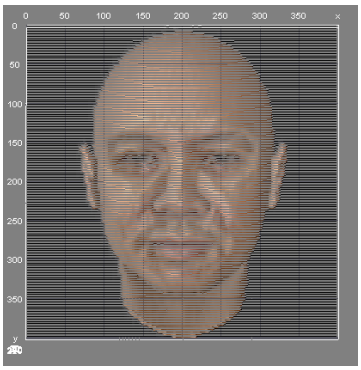

Fig. 1 Initial Facial Image 3D Surface Plot

When the control vertices are displaced, the Cartesian coordinates of the model are re-computed based on their previously calculated (s,t,u) values. This simple technique is quite effective at producing dramatic deformations, even for lattices of relatively few control vertices [17]. Conceptually, in another method by [18] was developed which used an initial lattice and B-spline control points to approximate the shape of the intended deformation. FFD is a powerful modeling tool because anything drawn inside of the initial, undeformed rectangle will experience the distortion. Denote by (Xmin, Ymin) and (Xmax, Ymax) the corners of a deformation region, and by m and n the degrees of the FFD function (there are m + 1 vertical columns and n + 1 horizontal rows of control points) [24]. FFD is a two-step process:

1. Compute the (s, t) coordinates for each point to be deformed. The s and t coordinates of a point in the deformation region range between 0 and 1 (see Figure 2). For a point in the rectangular region whose Cartesian coordinates are (x, y) as shown in Equation 3.

$$s = \frac{x - X_{min}}{X_{max} - X_{min}}, t = \frac{y - Y_{min}}{Y_{max} - Y_{min}}. \quad (3)$$

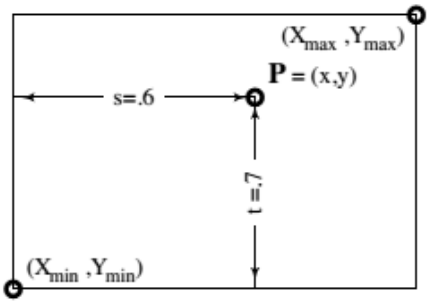

Fig. 2 FFD Local Coordinates

2. Compute the homogeneous coordinates X(s, t) = (X, Y, W) of the deformed point using the rational bivariate tensor product Bernstein polynomial equation as shown in Equation 4.

$$X(s,t) = \sum_{j=0}^{n} \sum_{i=0}^{m} B_i^m(s) B_j^n(t) P_{ij}. \quad (4)$$

where $B_i^n(t)$ and $B_j^m(s)$ are Bernstein polynomials and $Pij = wij\ (xij\ , yij\ , 1)$ are the homogeneous coordinates of the displaced control point i, j. Note that weights can be assigned to the FFD control points. If all weights wij=1 and if the control points form a rectangular lattice $P_{i,j} = (X_{min+}\frac{1}{m}(X_{max} - X_{\min}), Y_{min} + \frac{j}{n}(Y_{max} - Y_{min}))$, FFD is the identity transformation: all points end up where they started from. Points outside of the rectangle are not moved. If a shape is only partially inside the FFD region, one can control the degree of continuity between the deformed and undeformed portions of the shape by "freezing" rows of control points.

2.2 Image Homography

Many researchers had been proposing different methods to view perspective distortion from a single image. Murali [35] have proposed a method based on perspective transformation and plane homography to rectify the

perspective distortion in an image to actual scale. Liang [36] getting estimates shape from texture flow information obtained directly from the image without requiring additional metric data. The method needs neither high contrast document boundary nor paragraph formatting information. Hartley [23] uses methods of projective geometry to determine a pair of 2D projective transformations to be applied to the two images in order to match the epipolar lines. In computer vision, for any two images of the same planar surface in space are related by a homography. The images are prospective.

A 2D point (x, y) in an image can be represented as a 3D vector x = (x1, x2, x3) $x = \frac{x1}{x3}$ and $y = \frac{x2}{x3}$. Hartley also [37] provide the specific definition that a homography is an invertible mapping from P^2 to itself such that three points lie on the same line if and only if their mapped points are also collinear. The homography transformation has 8 degrees of freedom and there are other, simpler transformations that still use the 3×3 matrix but contain specific constraints to reduce the number of degrees of freedom. This section presents a hierarchy of transformations leading to the homography and will show how homographies can be broken down into an aggregation of these simpler transformations. This is discussed in much more detail in [38].

2.3 Radial Distortion Model

Several studies have shown the ways for making visible radial distortion in vision literature. The author mostly agree that only the first coefficient is required, even if parameters for higher order distortion are required numerical stability usually require that the second order term be found first, it also mentioned in [27] for an image centered around the origin, distorted points are denoted x_d and the calculated undistorted points as x_u as shown in Equation 5.

$$x_d = \frac{x_u}{(1-k\| x_u\|^2)} \qquad x_u = \frac{x_d}{(1-k\| x_d\|^2)}. \tag{5}$$

Fig. 3 Effect of radial distortion on image geometry

As shown in figure 3, this notation means that images are containing negative distortion, $\kappa < 0$, exhibit barreling and such images are corrected by applying positive distortion (and vice-versa for pin-cushion images). Note that this notation is equivalent to that of Tsai [11], Li and Lavest [6], Weng et al. [12] and others up to first order.

A geometric transformation is a kind of image processing operation that reformulates the spatial connection between points in an image. The size and shape of an image's layout can be manipulated and average distortion compensation of imaging sensors, calibration for image registration, geometrical normalization for image analysis. Piecewise interpolation has received much attention in the spline research work. The majority of the work, assuming the data is available on a rectangular grid. Instead of considering the problem of fitting a composite surface to scattered 3-D data [25]. The global polynomial transformations described earlier impose a single mapping function upon the whole image. They do not account for local geometric distortions such as scene elevation, atmospheric turbulence, and sensor nonlinearity.

Consequently, piecewise mapping functions have been introduced to handle local deformations [4]. B-splines methods are piecewise-polynomial bases with a low computational cost, and their approximation properties are optimal in a mathematically [6, 7, 22]. A deformation model based on B-splines is very versatile and can generate a large variety of nonlinear elastic deformations [8, 9, 10, 11]. The deformation field can be viewed as a set of several functions (one per coordinate) which in turn are modeled by a linear sum of weighted and shifted B-splines. The set of weights, which are called the B-spline coefficients, fully characterize the transformation [22]. This nonlinear elastic deformations deformation model can be produced while keeping a high control on its level of detail and ensures high-quality model interpolation [5]. So in this model radial distortion is where image points are displaced in a radial direction from the center of distortion.

2.4 Pincushion Deformation Model

Most computer vision algorithms have been relying on the assumption of a linear camera pinhole model. This introduces severe optical distortion from the pinhole assumption. Radial distortion is the most significant type of distortion [19, 21, 34]. Radial distortion bends straight lines into circular arcs violating the main invariance preserved in the camera pinhole model [1]. Radial distortion may appear as a pincushion distortion that is usually arising at longer focal lengths. Radial distortion is a non-linear transformation of the image increasing from the center of distortion to the periphery of the image [3]. The center of lens distortion is a point somewhere close to the center of the image, around which distortion due to the shape of the camera lens is approximately symmetrical. Two of the most common distortions are a barrel (k>0) and pincushion (k<0) distortions, where k is the distortion parameter which indicates the amount of lens radial.

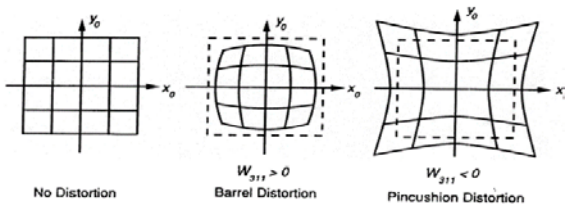

Fig. 2 Two of the most common distortions

The function from deformed images is $(r, k) = 1 + kr^2$, called radius (r) is the distance from the center of the image and k value is a determined constant which has a positive value for barrel images and a negative value for the pincushion distortion. The pinchusion distortions are visually most prominent at the image corners and sides [20]. In order to see the effect of the distortions on the integral projection vectors the barrel distorted grid image with k = 0.3 and the pincushion grid image with k = - 0.3 are used. It can be easily seen on Figure 4. that the projection vectors of the pincushion deformed images are starting from the center towards the whole images. The edges could help to detect the horizontal displacement through the integral projection vectors are lower.

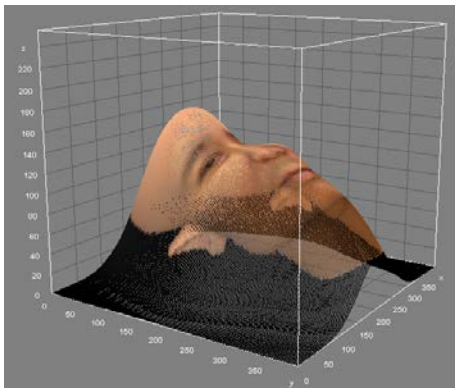

Fig. 5 Visualization projection from the facial image

The center of distortion is not in general in the center of the image. However, as the correct position is not well constrained, it is necessary to fix it somewhere, and the image center turns out to be a reasonable approximation as perspective as we have tested. In practice, the distortion is radial with aspect ratio and skew of the distortion are given by the camera calibration, which, as we will show, cannot be reliably estimated without correcting the distortion. So, we will adopt the approximation which most authors make (but few states) of assuming zero skew and aspect ratio close to unity, as this allows the distortion to be modeled as radial in the image. The two key observations we make here are that an essential, but usually implicit, the assumption in self-calibration algorithms for rotating cameras is that the 3D lines connecting matched features all intersect at the same fixed point in space — the rotation center. Radial distortion causes problems for such algorithms because these reconstructed “match-lines” no longer intersect at the rotation center. The effect can be seen in Figure 5 which shows cross sections of image planes as tangent planes to a sphere. If the image is distorted, then the image is displaced slightly.

2.5 Determining Image Quality

The traditional techniques that are mainly used are Mean Squared Error (MSE) and Peak Signal to Noise Ratio (PSNR) for error measuring. These are widely used because they are simple to calculate and are independent of viewing conditions and individual observers. Quality index, on the other hand, is designed by modeling any image distortion as a combination of three factors: loss of correlation, luminance distortion, and contrast distortion. It performs significantly better than the widely used distortion metric mean square error. The peak signal-to-noise ratio (PSNR) is obtained by dividing the peak power by Minkowsky metrics. It is an engineering term for the ratio between the maximum possible power of a signal and the power of corrupting noise that affects the fidelity of its representation [30].

Because many signals have an extensive dynamic range, (ratio between the most significant and smallest possible values of a changeable quantity) the PSNR is usually expressed regarding the logarithmic decibel scale. Based on the assumption that image quality degradation comes from the error between image pixels, the Peak Signal to Noise Ratio (PSNR) is one of the standard methods for image quality evaluation, that is used for image quality metrics and defined as the ratio of the signal, where the signal is the reference image to the noise.

MSE is a signal fidelity measure. The goal of a signal fidelity measure is to compare two signals by providing a quantitative score that describes the degree of similarity/ fidelity or, conversely, the level of error/distortion between them. Usually, it is assumed that one of the signals is a pristine original, while the other is distorted or contaminated by errors.

Suppose that x = { xi |i = 1, 2, · · · , N} and y = { yi |i = 1, 2, · · · , N} are two finite-length, discrete signals (e.g., visual images), where N is the number of signal samples (pixels, if the signals are images) and xi and yi are the values of the i th samples in x and y, respectively. The MSE between the signals x and y as shown in Equation 6.

$$MSE(x, y) = \frac{1}{N}\sum_{i=1}^{N}(x_i - y_i)^2 . \quad (6)$$

In the MSE, it often refers to the error signal ei,= xi − yi, which is the difference between the original and the distorted one. If one of the signals came from an original signal quality, and the other one is a distorted version of it whose quality is being evaluated, then the MSE will be

regarded as a measure of signal quality. A general form function as shown in Equation 7.

$$d_p = (x, y) = (\sum_{i=1}^{N} |e_i|^p)^{1/p}. \quad (7)$$

MSE is often converted into a peak-to-peak signal-to-noise ratio (PSNR) measure as shown in Equation 8.

$$PSNR = 10log_{10} \frac{L^2}{MSE}. \quad (8)$$

Where L is the dynamic range of allowable image pixel intensities. For example, for images that have allocations of 8 bits/pixel of gray-scale, L = $2^8 - 1 = 255$. When pixels are represented using 8 bits per sample, this is 255. For color images with three RGB values per pixel, the definition of PSNR is the same except the MSE is the sum over all squared value differences divided by image size and by three. Studies of the [28] Video Quality Expert Group (VQEG) have shown that the PSNR measure is an excellent indicator of subjective preference in video coding [30]. The PSNR is useful if images having different dynamic ranges are being compared, but otherwise contains no new information relative to the MSE. Due to MSE has many attractive features, the MSE's criterion can be developed when considering a smooth loss function in a neighborhood parameter. Three Considering why using MSE, and its led to: First, Parameter-free with complexity additions per sample. MSE become inexpensive to compute because it is memoryless and the squared error can be evaluated from each sample, and also independent of other samples. Second, Define the energy of the error signal. MSE being an energy measure to preserved after any orthogonal (or unitary) linear transformation, such as the Fourier transform. MSE energy property guarantees that the energy of signal distortion in the transform domain is the same as in the signal domain [29]. Third, Become the first metric in the context of optimization. Minimum-MSE (MMSE) optimization problems often have closed-form analytical solutions, and when they do not, iterative numerical optimization procedures are often easy to formulate, since the gradient and the Hessian matrix [32] of the MSE are easy to compute.

3. Methods

From a practical point of view, it is more convenient to approximate the target image and warped image. We used to concentrate our attention on regions of interest within the source and target images. Let us call the regions of interest of the source and target images, respectively. Then, we measure the dissimilarity between the warped source image and the target image where defines a mask typical to the source and target images and the size of the mask in pixels. The dissimilarity point is sensible to linear transformations of the gray image values, and the deformation field may be different if the gray values are transformed in one of the images. Barrel or pincushion distortions are so-called radial distortions. The simplest way to model this effect is with a shift to the pixel coordinates. The radial shift of coordinates modifies only the distance of every pixel from the image center. Let r denote the distance of the undistorted image coordinates from the center. Let $\bar{q} = (x_n, y_n)^T$ represents undistorted coordinates, while $= (x_d, y_d)^T$ represents coordinates in the deformed an image. Every radially symmetric distortion may be approximated using Taylor series in the following form as shown in Equation 9.

$$\emptyset(r^2) = 1 + K1r^2 + K2r^4 + \cdots, \quad (9)$$

Where $r^2 = \bar{x}^2 + \bar{y}^2$ a $K1, K2$ are coefficients of radial distortion.

To have these coordinates independent of image dimensions, the coordinates $\bar{x}$, $\bar{y}$ are dimensionless. Moreover, to preserve radial symmetry, we must move the origin of the coordinate system to the center of the image. Coordinates of required properties can be obtained using the following formula as shown in Equation 10.

$$\bar{x} = \frac{x_n - c_u}{R} \qquad \bar{y} = \frac{y_n - c_V}{R}. \quad (10)$$

For $R = \sqrt{c_u^2 + c_v^2}$ and coordinates of the center of the image $c_u = \frac{w}{2}$, $c_v = \frac{h}{2}$ (w is width and h height of image). Resulting transformation from coordinates xn, yn of reconstructed image to the coordinates xd, yd of original deformed image can be written using the following formula as shown in Equation 11.

$$\begin{pmatrix} x_d \\ y_d \end{pmatrix} = \begin{pmatrix} x_n - c_u \\ y_n - c_v \end{pmatrix} \emptyset^{-1}(r^2) + \begin{pmatrix} c_u \\ c_v \end{pmatrix}. \quad (11)$$

We go pixel by pixel of the output image $(x_n, y_n)^T$ and compute corresponding pixel coordinates in input image $(x_d, y_d)^T$. These coordinated are in general real numbers, so we have use a valid interpolation method, e.g., nearest neighbour. To achieve better result, use bilinear interpolation. Result obtained using described method is shown in Figure 6.b, 6.c, 6.d.

4. Results

The image generation of any kind of camera – like film or CCD cameras – may be modeled with the pinhole camera model. However, the images of real cameras suffer from more or less lens distortion, which is a nonlinear and generally radial distortion. The most prevalent form of this

effect is the barrel and the pincushion distortion. The first is because many wide angle lenses have higher magnification in the image center than at the periphery. This cause the image edges to shrink around the center and form a shape of a barrel. The pincushion distortion is the inverse effect when the edges are magnified stronger (see figure 6.d). There are different situations using image processing and computer vision algorithms or creating special effects, where the lens distortion is not acceptable.

Fig. 6.a Initial 3D facial Data

Fig. 6.b with parameters κ1 = 0 and κ2 = 1 some pixels are moved to multiple positions

Fig. 6.c with parameters κ1 = 1 and κ2 = 2 some pixels are moved to multiple positions

Fig. 6.d with parameters κ1 = 1 and κ2 = 3 the facial image deformed

The value of the signal–to–noise ratio, SNR, this value can have several definitions. The SNR value or more likely the noise is characterized by its standard deviation. It also can differ if the signal is known to lie between two boundaries, $a_{min} \leq a \leq a_{max}$, and then the SNR as shown in Equation 12.

$$SNR = 20log_{10}\left(\frac{a_{max}-a_{min}}{std.deviation}\right). \quad (12)$$

In an actual observation, the noise fluctuation is very often measured in a quantized level form at a discrete time interval. In this case, it increases in importance, especially from a methodological viewpoint, to establish a unified statistical treatment for evaluating the L_{eq} noise evaluation index, and to develop a signal processing method for the reduction of level quantization errors.

Table 1: Tabulated result

Param	SNR	PSNR	RMSE	MAE
κ1 = 0; κ2 = 1	9.338424	16.313903	29.5027238	10.5450952
κ1 = 1; κ2 = 2	3.996214	10.971689	54.5723698	32.1266306
κ1 = 1; κ2 = 3	3.410667	10.386142	58.3781284	35.9175127
κ1 = 2; κ2 = 3	2.923990	9.899470	54.5723698	32.1266306
κ1 = 3; κ2 = 2	2.479110	9.454590	64.9871918	43.0463493
κ1 = 3; κ2 = 1	1.863934	8.839413	69.7568175	48.9409058

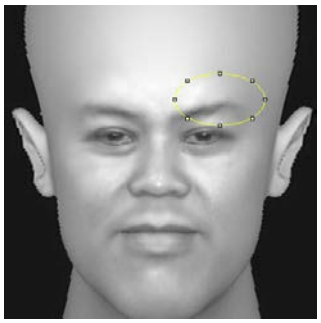

Fig. 7 The noise is the same over the entire image

5. Conclusion

Image model deformation has been representing with appropriate approach and objects which have similar structures can be adequately modeled using this algorithm. Generic models can be created from scratch and refined by changing constraint on k value over many models, tabulated result shown in Table 1. As demonstrated, using this method can be applied to generate models of human faces. Full head models have also been creating by modifying the generic model applied to the input images. In applications where it is difficult or expensive to obtain accurate estimates of the 3D structure of an object directly, a subset of features can be located, and a default model can be adapted to fit the surface in the least squares sense as shown in Figure 7.

Pin-Cushion distortion results in line intersections which are contained in a small area centered between the artificial camera center and the images. They will produce a self-consistent estimate, and so pin-cushion distortion will cause under-estimates of focal length as shown in Figure 8. With assumptions when using MSE, signal fidelity is independent of temporal or spatial relationships between the samples of the original signal. So, if the original and distorted signals are randomly re-ordered in the same way, then the MSE between samples and the original signal will be unchanged.

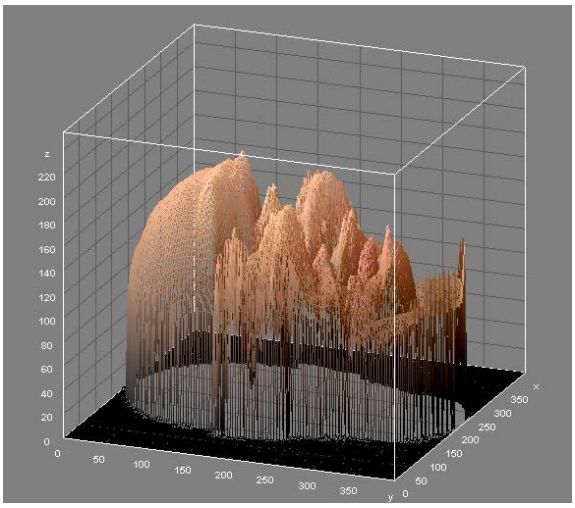

Fig. 8 Artificial visualization from the facial image with 3D mesh with smoothing factor = 11.5 and scaling perspective value = 0.22

For a given error signal, the MSE remains unchanged, regardless of which original signal it is added to. Unfortunately, not one of them holds (even roughly) in the context of measuring the visual perception of image fidelity. Dramatic visual examples of the failure of the MSE concerning the veracity of these assumptions is demonstrated.

Acknowledgment

The authors would like to express their cordial thanks to Pak Nemuel Daniel Pah, Ph.D. for his valuable advice.

References

[1] Wang, A., Qiu, T., Shao, L, (2009) A simple method of radial distortion correction with the center of distortion estimation. Journal of Mathematical Imaging and Vision 35(3), 165–172.

Huang, J., Shi, X., Liu, X., Zhou, K., Wei, L., Teng, S., Bao, H., Guo, B., and Shum, H.Y, (2006) Subspace gradient domain mesh deformation. ACM Trans. Graph. 25, 3, 1126–1134.

Bukhari, F., Dailey, M., Automatic Radial Distortion Estimation from a Single Image., Journal of Mathematical Imaging and Vision manuscript.

Goshtasby, A.,(1986) Piecewise Linear Mapping Functions for Image Registration," Pattern Recognition, vol. 19, no. 6, pp. 459-466.

M. Unser, A. Aldroubi, and M. Eden, (1991) Fast B-spline transform for continuous image representation and interpolation," IEEE Trans. Pattern Anal. Mach. Intell., vol. 13, no. 3, pp. 277–285.

M. Unser, (1999) Splines: A perfect fit for signal and image processing," IEEE Signal Process. Magazine, vol. 16, no. 6, pp. 22–38.

E. Meijering, W. Niessen, and M. Viergever, (2001) Quantitative evaluation of convolution-based methods for medical image interpolation," Med.Image Anal., vol. 5, no. 2, pp. 111–126.

D. Mattes, D. R. Haynor, H. Vesselle, T. K. Lewellen, and W. Eubank, (2003) PET-CT image registration in the chest using free-form deformations, IEEE Trans. Med. Imag., vol. 22, no. 1, pp. 120–128.

J. Kybic and M. Unser, (2003) Fast parametric elastic image registration," IEEE Trans. Image Process., vol. 12, no. 11, pp. 1427–1442.

R. Szeliski and H.-Y. Shum, "Motion estimation with quadtree splines, (1996) IEEE Trans. Pattern Anal. Mach. Intell., vol. 18, no. 12, pp. 1199–1210.

O. Musse, F. Heitz, and J.-P. Armspach, (2003) Fast deformable matching of 3D images over multiscale nested subspaces. Application to atlas-based MRI segmentation," Pattern Recogn., vol. 36, no. 8, pp. 1881–1899.

Botsch, M., and Kobbelt, L. Real-time shape editing using radial basis functions. Eurographics 2005.

Lipman, Y., Sorkine, O., Levin, D., and Cohen, D, (2005) Linear rotation-invariant coordinates for meshes. ACM Trans. Graph. 24, 3, 479–487.

Liu, Zhang, Huang and Tan, Deformable Object Matching via Deformation Decomposition based 2D Label MRF, CVPR. 2014

A.H. Barr. Global and Local Deformations of Solid Primitives. Proceedings of the SIGGRAPH 84 (Page: 21-30 Year of Publication: 1984).

Sederberg, T. W., and Parry, S. R., Free-Form Deformation of Solid Geometric Models, Proceedings of the SIGGRAPH 86, Computer Graphics 20 (Page: 151-159 Year of Publication: 1986).

Draper and Egbert. A Gestural Interface to Free-Form Deformation., Brigham Young University

Coquillart, S., Extended Free-Form Deformation: A Sculpturing Tool for 3D Geometric Modeling, Proceedings of the SIGGRAPH '90, Computer Graphics 24, 4 (Page: 187-196 Year of Publication: 1990).

Kukelova, Z., Pajdla, T, (2011) A minimal solution to radial distortion autocalibration. IEEE Transactions on Pattern Analysis and Machine Intelligence 99(1).

Albu F and Corcoran P., Transformed Integral Projection Method for Global Alignment of Second Order Radially Distorted Images Strand, R., Hayman, E.: Correcting radial distortion by circle fitting. In: British Machine Vision Conference (BMVC) (2005)

Sorzano, Thévenaz, Unser., (2005) Elastic Registration of Biological Images Using Vector-Spline Regularization, IEEE TRANSACTIONS ON BIOMEDICAL ENGINEERING, VOL. 52, NO. 4.

Richard I. Hartley, "Theory and Practice of Projective Rectification", International Journal of Computer Vision No.2, (Page:115-127 vol 35, Year of Publication 1999).

Thomas W. Sederberg. COMPUTER AIDED GEOMETRIC DESIGN. (2003) 149-151.

Franke, R., "A Critical Comparison of Some Methods for Interpolation of Scattered Data. "Naval Postgraduates School Technical Report, NPS-53-79-003, 1979.

Zhizhong Zhe, Hong Ren Wu, A New Way of Pooling: Starting from An Image Quality Measure, Proceedings of the IEEE on signal processing (Page: 1080 - 1083 vol.2, Year of Publication: 2004)

Murray, Tordoff, Violating Rotating Camera Geometry: The Effect of Radial Distortion on Self-Calibration

VQEG, " Final report from the video quality experts group on the validation of objective models of video quality assessment.", 2000.

Z. Wang and A. C. Bovik, “Mean squared error: love it or leave it? - A new look at signal fidelity measures,” IEEE Signal Processing Magazine, vol. 26, pp. 98-117, Jan. 2009.
J. H. Jeong, Analysis and Visualization of Multi-mode Optical Spectral-signature Bioimaging Data for In Vivo Applications, Ph.D. Thesis, Biomedical Engineering, University of Southern California, 2007.
Z. Wang and A. C. Bovik, (2006) Modern Image Quality Assessment. Morgan and Claypool Publishing Company, NewYork.
M.P Eckert and A.P. Bradley,” Perceptual quality metrics applied to still image compression,” Signal Processing, vol.70, pp.177-200, Nov. 1988.
T. M. Galla, Cluster Simulation in Time-Triggered Real-Time Systems, Ph.D. Thesis, Dept. Computer Engineering, University of Technology, Vienna, Austria, 1999.
Zhang, Z, (2000) A flexible new technique for camera calibration. IEEE Transactions on Pattern Analysis and Machine Intelligence 22(11), 1330–1334
Murali.S (2008) “Rectification of Perspective distortion using camera parameters - A Perspective Geometry Based Approach”, ICGST International Journal on Graphics, Vision and Image Processing, GVIP, Vol 8, pp.1-7.
Liang (2008) “Geometric Rectification of Camera-Captured Document Images”, IEEE Transactions On Pattern Analysis And Machine Intelligence, Vol.30, No.4, pp 591-605.
Hartley, “Multiple View Geometry in Computer Vision”. Cambridge University Press, second edition, 2003.
Dubrofsky, “Homography Estimation”, 2009

Cahyo Darujati received a bachelor in 2004 and master degree in 2010 respectively from Electrical Engineering Department, Institut Teknologi Sepuluh Nopember, Surabaya, Indonesia. He is a Professional Lecturer Faculty of Computer Science, Narotama University, Surabaya, Indonesia. His research interest includes computer vision, image processing, and video processing. He is IAENG member.
(e-mail: cahyo11@mhs.ee.its.ac.id)

Bimo Gumelar, Fulltime Lecturer Faculty of Computer Science, Narotama University and Professional Researcher in Neuroscience Computing and Human-Computer Interaction, specialized in Auditory Cognitive Modelling Using Neuromorphic Platform. He is responsible for the Human-Computer Interaction and Research Methodology course.
(E-mail: bimo.gumelar@narotama.ac.id)

Supeno Mardi Susiki Nugroho graduated from Electrical Engineering Institut Teknologi Sepuluh Nopember (ITS), Surabaya, Indonesia for his bachelor in 1995 and received master and doctoral degree in 2003 and 2013 respectively from Electrical Engineering of Institut Teknologi Sepuluh Nopember (ITS), Surabaya, Indonesia. He is currently a lecturer of Electrical Engineering Department ITS. His research interest includes image processing, computer network, and Artificial Intelligence.
(E-mail: mardi@ee.its.ac.id)

Mochamad Hariadi received the B.E.degree in Electrical Engineering Department of from Institut Teknologi Sepuluh Nopember, Surabaya, Indonesia, in 1995. He received both M.Sc. and Ph.D. degrees in Graduate School of Information Science Tohoku University Japan, in 2003 and 2006 respectively. Currently, he is a staff of the Electrical Engineering Department of from Institut Teknologi Sepuluh Nopember, Surabaya, Indonesia. He is the project leader in joint research with PREDICT JICA project in Japan.
(e-mail: mochar@ee.its.ac.id).